Journal of Non-Crystalline Solids 382 (2013) 24–31

Contents lists available at ScienceDirect

Journal of Non-Crystalline Solids

journal homepage: www.elsevier.com/ locate/ jnoncrysol

EXAFS study of changes in atomic structure of silver nanoparticles in soda-lime glass caused by annealing

Vasiliy V. Srabionyan [a], Aram L. Bugaev [a], Vasiliy V. Pryadchenko [a], Alexander V. Makhiboroda [a], Elizaveta B. Rusakova [a], Leon A. Avakyan [a], Reinhard Schneider [b], Manfred Dubiel [c], Lusegen A. Bugaev [a,*]

[a] Physical Department, Southern Federal University, Zorge str.,5, Rostov-on-Don 344090, Russia
[b] Karlsruhe Institute of Technology, Kaiserstraße 12, D-76131 Karlsruhe, Germany
[c] Department of Physics, University of Halle-Wittenberg, Von-Danckelmann-Platz 3 D-06120 Halle, Germany

ARTICLE INFO

Article history:
Received 19 July 2013
Received in revised form 24 September 2013
Available online 22 October 2013

Keywords:
Silver nanoparticles in glass;
Annealing;
Atomic structure;
Mechanism of nanoparticle growth;
Extended X-ray absorption fine structure

ABSTRACT

Atomic structure of silver nanoparticles in soda-lime glass at T = 10 K before and after annealing was studied by Ag K-edge EXAFS. To overcome ambiguities in the structure determination by the Fourier-transform analysis of these spectra, caused by the presence of various species of the absorbing silver atoms in the sample, the refinements of the fitting technique of the Fourier transforms F(R) have been implemented. The F(R) of Ag K-edge EXAFS in as prepared and annealed glasses were analyzed in the extended range of interatomic distances (R) up to ~6.5 Å using Ag K-edge EXAFS in Ag-foil at the same temperature as the reference. The proposed technique of the fit enabled to go beyond the averaged description of silver nanoparticles structure in glass and to reveal the atomic structure of the core region of nanoparticles, the structural characteristics of their near-surface region, parameters of Ag – O bonds inside the glass matrix and the percentage of Ag atoms in each of these species before and after the annealing process. The mean size of silver nanoparticles in as prepared and annealed glasses was estimated and the mechanism of nanoparticles growth after the thermal treatment was suggested.

1. Introduction

Silver nanoparticles are extensively used as catalysts, bactericidal agents, in the production of anti-reflective optical coatings [1–3]. The size of nanoparticles, structure and composition of their interior and the near-surface regions determine the exhibited properties. Therefore silver nanoparticles have been studied by different experimental and theoretical techniques including X-ray absorption spectroscopy (XAS), to establish the dependence of size and atomic structure on the treatment conditions, kind of the stabilizing matrix or the support [4–9]. The XAS method is especially promising for such a structural analysis since experimental spectra of nanoparticles, differently prepared or existed in different surroundings, differ essentially from each other and from the spectra of corresponding bulk compounds. Interpretation of the observed differences in spectra and their numerical analysis enables to get the required structural information. However, the obtained information dominantly has an averaged character because the absorbing Ag atoms in the studied material are often existed in a several species, differed by the type of Ag local structure. Therefore, determination of atomic structure in metallic silver nanoparticles, including the type of point symmetry in the interior (core) region of small nanoparticles, the nearest-neighbor Ag–Ag distances and the structure of the near-surface region still remain a challenging problem.

In this paper XAS is applied to determine the atomic structure of silver nanoparticles in soda-lime glasses at temperature $T = 10$ K and the structural changes, caused by the thermal treatment (annealing) during 8 h at $T = 823$ K [10]. To get structural information of the core and near-surface regions of silver nanoparticles the Fourier-transform (FT) analysis of experimental Ag K-edge extended X-ray absorption fine structure (EXAFS) in “as prepared” and “annealed” glasses was performed. The application of this technique to materials with various local structures of the absorbing atom requires a large number of variables, which are often strongly correlated. The fit results depend also upon the wave numbers interval $\Delta k = k_{max} - k_{min}$, used for the Fourier-transformation of the oscillatory part $\chi(k)$ of experimental EXAFS, and hence Δk must be considered as one of the factors, which affects the outcome. As a result, the fitting procedure becomes unstable and normally gives only the average values of the limited number of structural parameters. To overcome these difficulties and limitations in the structural analysis of nanoparticles by EXAFS we propose in Section 3 the refinements of the fitting procedure which enabled to perform the structural analysis of silver nanoparticles under the presence of different species of Ag atoms in glass. In Section 4 this fitting procedure is applied to Ag K-edge EXAFS in as prepared and annealed samples to determine the atomic structure of the core region in silver nanoparticles, the average values of structural Ag–Ag parameters for

* Corresponding author. Tel.: +7 863 297 53 36; fax: +7 863 297 51 20.
E-mail address: bugaev@sfedu.ru (L.A. Bugaev).

0022-3093/$ – see front matter © 2013 Elsevier B.V. All rights reserved.
http://dx.doi.org/10.1016/j.jnoncrysol.2013.09.025

their near-surface region, as well as to determine the percentage of Ag atoms in the core, near-surface regions of nanoparticle and of Ag ions bonded with two oxygen atoms in glass matrix. The obtained structural parameters were used to estimate the change of silver nanoparticles mean size and to propose the mechanism of nanoparticle growth after the thermal treatment.

2. Experimental

Soda-lime-silica glasses containing (in wt.%) 70.95% SiO_2, 14.1% Na_2O, 8.4% CaO, 3.69% MgO, 1.8% Fe_2O_3, 0.6% Al_2O_3, 0.18% K_2O and 0.22% SO_3 have been used as base glass material. Ag ions were introduced into by an Ag/Na ion exchange of several slices (15 mm × 15 mm in square and about 150 μm thick) of the base glass in a $NaNO_3$/0.05% $AgNO_3$ melt at 603 K for 195 h. Experiments of energy-dispersive X-ray spectroscopy (EDXS) of cross-section specimens showed a silver/sodium of approximately 10% at the glass surface immediately after the ion exchange (as-prepared). EDXS results demonstrated that the silver content decreases continuously from each surface side down to a depth of about 50 μm. In the glass interior no Ag could be detected, while upon annealing at 603 K a constant amount of silver was found throughout the whole sample as a result of interdiffusion processes.

Transmission electron microscope (TEM) investigations were carried out in addition to evaluate the size of silver particles by means of a Philips CM 20 FEG at 200 kV. Typical TEM bright-field images taken from different deep regions of the as-prepared sample and the annealed one, respectively, can be seen in Fig. 1. Obviously, compared to the initial state after annealing an increased number of Ag particles is present (Fig. 1c,d). For both charges of samples similar values of the particle size were measured in surface-near regions (as prepared: 1.5–6.5 nm, annealed: 1.5–5 nm). However, significant differences in the area density of nanoparticles can be observed. Presumably, the thermal treatment predominantly promoted nucleation processes, thus leading to an increase of the number of particles. Generally, for both samples the average particle size increases as a function of depth. In addition, in the case of the as-prepared state the number of Ag particles drops down drastically in regions deeper than about 50 μm. In the middle of this sample nearly no particles are present (see Fig. 1b). This is in contrast to the annealed sample, exhibiting a few particles with sizes up to 30–40 nm besides smaller ones in interior zones (cf. Fig. 1d). These TEM images do not demonstrated the existence of core–shell structures reflecting different densities of silver atoms within the silver particles. Some high-resolution TEM investigations showed similar results representing the structure of monocrystalline or polycrystalline Ag particles.

In HASYLAB (Hamburg, Germany) at beamline X1 Ag K-spectra (25.514 keV) were recorded in transmission mode at 10 K by means of a liquid-helium vapor flow cryostat. In each case a stack of several glass slices was used as sample in order to get a sufficient high signal. Experimental Ag K-edge EXAFS spectra of silver metallic foil as reference and of as prepared and annealed ion-exchanged soda-lime glasses for 8 h at 823 K were recorded [10].

3. Theory. Data analysis method

To study atomic structure of as prepared and annealed soda-lime glasses by experimental Ag K-edge EXAFS spectra one must consider at least two Ag species (states), contributing into oscillatory parts $\chi(k)$ of these spectra: i) Ag atoms in silver nanoparticles and ii) Ag ions inside the glass matrix, connected with two oxygen atoms, similar to that in AgO [11]. In Fig. 2 $\chi(k)$ of experimental Ag K-edge EXAFS and their Fourier-transforms F(R) in as prepared and annealed samples at $T =$ 10 K are compared to those of Ag K-edge EXAFS in Ag foil at the same temperature. Fig. 2(a) shows that the amplitudes of $\chi(k)$ oscillations in the spectra of glasses are lowered in comparison to foil, reducing the k-interval of the useful signal to $k_{max} \sim 14\,\text{Å}^{-1}$ for as prepared sample. Moreover, there are no significant changes in the frequencies of $\chi(k)$ oscillations beginning from $k \sim 4\,\text{Å}^{-1}$ to k_{max}. Fig. 2(b) shows that in the extended R-range of interatomic distances, all the peaks in $F(R)$ of Ag foil are retained in $F(R)$ of glasses. For Ag foil these peaks are reproduced below in Fig. 4(b) by the fit, taking into account the first five coordination shells of Ag in *fcc* structure of Ag foil and therefore, the comparison of Fig. 2(b) indicates that at least part of Ag atoms in nanoparticles, existing in as prepared and annealed glasses, have a local structure similar to that of *fcc* in Ag foil.

The simplest model of nanoparticles atomic structure, that provides such a behavior of $F(R)$ in the extended R-range, could be the atomic cluster of a chosen size, with undistorted *fcc* structure up to the cluster's surface. However, on the real surface and in the few following atomic layers the concentration of defects increases [12] and as the next approximation it is reasonable to assume that the model of silver nanoparticle atomic structure should consist of the *fcc* core and the near-surface region, which includes the atoms of the surface and subsurface layers. The last one should be a more or less distorted *fcc* structure with regard to atom positions and lattice vibrations. According to this model one must consider the following species (states) of the absorbing Ag atoms in glass, schematically illustrated in Fig. 3: Ag(1)—atoms in the core region of nanoparticle, which have the local structure similar to *fcc* structure of Ag foil; Ag(2)—atoms in the near-surface region of nanoparticle; Ag(3)—ions in glass bonded with two oxygen atoms.

Such a treatment permits to perform more detailed study of Ag nanoparticles atomic structure in soda-lime glasses using the fit of $F(R)$ of experimental Ag K-edge EXAFS, based on the function $\chi_{model}(k)$ compiled of the different terms $\chi_{Ag(i)}(k)$:

$$\chi_{\text{model}}(k) = C_1\chi_{Ag(1)}(k) + C_2\chi_{Ag(2)}(k) + C_3\chi_{Ag(3)}(k) \quad (1)$$

where each term $\chi_{Ag(i)}(k)$ represents the possible local structure of Ag(i) atom in glass. In this equation C_1, C_2, and C_3 are the percentages of Ag(1), Ag(2) and Ag(3) atoms respectively, from the total number of Ag atoms in glass, contributing to the $\chi(k)$ extracted from the experimental spectrum, so that:

$$C_1 + C_2 + C_3 = 1. \quad (2)$$

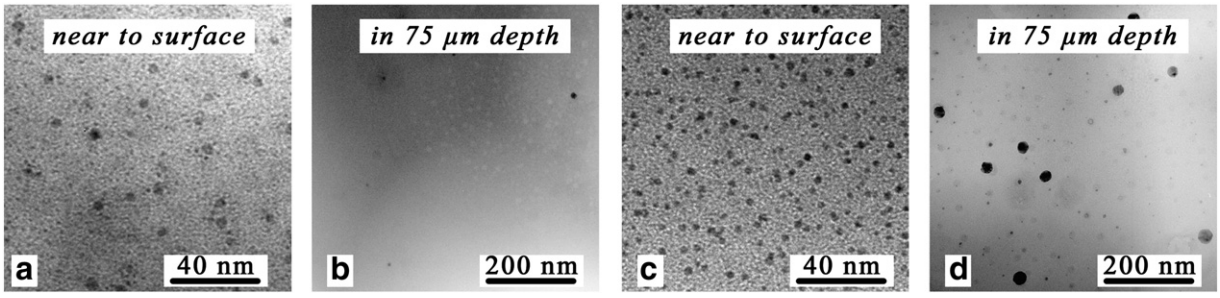

Fig. 1. TEM bright-field images of glasses with embedded Ag nanoparticles, microstructural peculiarities as found in different depths of a), b) the as-prepared sample, and c), d) the annealed one.

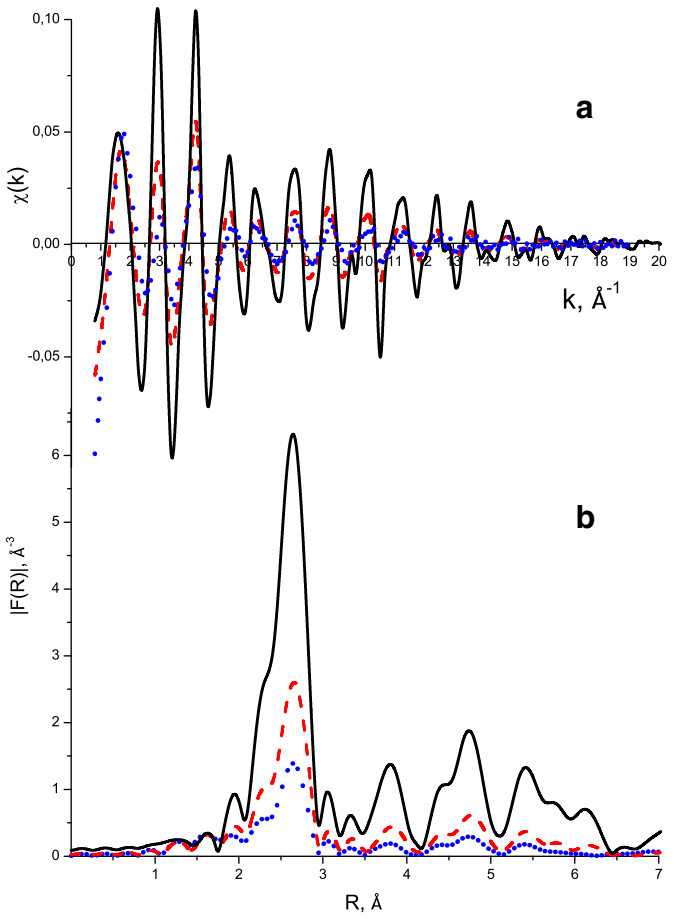

Fig. 2. Oscillatory parts $\chi(k)$ of experimental Ag K-edge EXAFS spectra (a) and corresponding FT magnitudes $F(R)$ of $k^2\chi(k)$ (b) in Ag foil (solid black curves), in annealed (dashed red curves) and in as prepared (dotted blue curves) soda-lime glasses at $T = 10$ K. FT was performed using the Δk range from $k_{min} = 2.8$ Å^{-1} to $k_{max} = 14.0$ Å^{-1}.

The term $\chi_{Ag(2)}(k)$ in Eq. (1) takes into account the interaction between neighboring Ag(2) atoms in the near surface region ($\chi_{Ag(2)-Ag(2)}(k)$) and interaction of Ag(2) atoms at nanoparticles surface with nearest oxygen ions of glass matrix, and therefore can be represented as:

$$\chi_{Ag(2)}(k) = \chi_{Ag(2)-Ag(2)}(k) + \widetilde{C}_2\chi_{Ag(2)-O}(k) \quad (3)$$

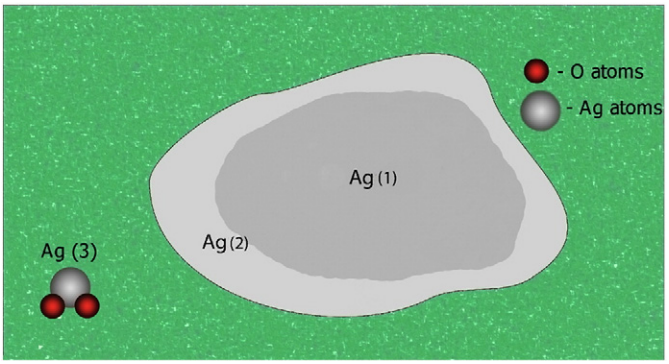

Fig. 3. Schematic picture, which illustrates different species (states) of the absorbing Ag atoms in glass: Ag(1)—atoms in the core of nanoparticle; Ag(2)—atoms in the near-surface region of nanoparticle; Ag(3)—ions bonded with two oxygen atoms. Background (green)—matrix of soda-lime glass.

where $\chi_{Ag(2)-O}(k)$ is the contribution of one atomic pair that consists of Ag(2) atom of nanoparticle and O ion of glass matrix; $\widetilde{C}_2$ is the multiplication of the fraction of Ag(2) atoms, which are bonded with O ions of matrix, and the number of such Ag(2) – O bonds.

With high probability one may expect that the contribution of Ag(2) atoms at nanoparticles surface which interact with O ions of glass matrix is negligible because of the following reason. From the comparison of F(R) of experimental Ag K-edge EXAFS presented in Fig. 2(b) the studied silver nanoparticles have a crystalline structure of neutral Ag atoms. Therefore, there are no strong interactions between the Ag(2) atoms of nanoparticles surface and O ions of amorphous matrix. In this case, the bond distances between these neutral Ag(2) atoms and O ions of glass should be much larger than ~2.17 Å, expected for Ag(3) – O bonds, and much more distributed.

Nevertheless, if we assume that some of Ag(2) atoms of nanoparticles surface are existed as the ions, interacting with O ions of glass, then one can show (see below) that the contribution of such Ag(2) – O bonds is smaller than the accuracy of C determination and therefore can also be neglected. Eq. (1) for this purpose can be simplified if we use reasonable assumption that the parameters of such Ag(2) – O bonds are the same (except the number of nearest O ions) as for Ag(3) states with the two nearest oxygen neighbors. In this case, using the above definition of $\chi_{Ag(2)-O}(k)$, the relation between this term and $\chi_{Ag(3)}(k)$ can be written as: $\chi_{Ag(2)-O}(k) = \chi_{Ag(3)}(k)/2$. By this relation we can rewrite Eq. (1) as:

$$\chi_{model}(k) = C_1\chi_{Ag(1)}(k) + C_2\chi_{Ag(2)-Ag(2)}(k) + C_{Ag-O}\chi_{Ag(3)}(k) \quad (4)$$

where

$$C_{Ag-O} = C_3 + C_2\widetilde{C}_2/2. \quad (5)$$

To perform Ag K-edge EXAFS analysis of soda-lime glasses using the considered structural model, the following changes in the FT technique and refinements of the fitting procedure were proposed.

The first is the choice of the k_{min} for FT at ~6.5 Å^{-1} (E ~ 25.663 keV), which enables i) to diminish the effect of photoelectron multiple scattering (MS) processes, essential in the structural analysis of Ag foil [13], and ii) to neglect the effect of Ag – O bonds on the values of Ag–Ag parameters in as prepared and annealed glasses determined by Δk interval started from this value of k_{min}. According to the results of [14] on the applicability of the existing criteria for signal frequencies resolution to the problem of close interatomic distances determination by the FT and fitting procedures applied to energy restricted X-ray absorption spectra, thus truncated Δk intervals (from k_{min} ~ 6.5 Å^{-1} to k_{max} ~ 14 Å^{-1} for as prepared sample and from k_{min} ~ 6.5 Å^{-1} to k_{max} ~ 18.5 Å^{-1} for the annealed one) provided the possibility to distinguish two models of Ag local structure with a difference in Ag–Ag distances larger than 0.015 Å. For Ag foil the FT over this Δk interval from k_{min} ~ 6.5 Å^{-1} to k_{max} ~ 14.0 Å^{-1} (the last was reduced to its value for $\chi(k)$ in as prepared glass) and the fit were performed using the third and the fourth cumulants in the expansion of the Debye–Waller (DW) factor in a power series of k [15]. In agreement with [16] these cumulants, needed to obtain high accuracy of Ag–Ag distances in Ag-foil at higher temperatures, appeared negligible at $T = 10$ K. The results of the fits of $F(R)$ in the R-range from 1.0 Å to 3.0 Å, presented in Table 1, were obtained by the two sets of backscattering amplitudes and phase shifts calculated by: i) Heddin–Lundqvist (HL) exchange-correlation potential model embedded in IFEFFIT package [17] and ii) Hartree–Fock (HF) exchange potential model [18]. The HF backscattering amplitudes and phase shifts were employed into the fit by making the corresponding replacements in the input files of IFEFFIT. Table 1 shows that the two models of potential for photoelectron provide approximately the same values of output parameters, yielding R_{Ag-Ag} in agreement with its X-ray diffraction (XRD) value and the physically reasonable value of the DW parameter $\sigma^2(Ag - Ag)$ at $T = 10$ K, which is in agreement with the earlier

Table 1
Structural parameters of the first shell of Ag in Ag foil at $T = 10$ K obtained by FT of Ag K-edge EXAFS and the single shell fit. FT of spectra was performed over Δk interval from ~6.5 to ~14.0 Å^{-1}, using HF and HL potentials for photoelectron backscattering amplitudes and phase-shifts calculation. The goodness of the fit is characterized by the reduced mean square deviation χ^2_ν [21].

Exchange-correlation potential for photoelectron scattering	χ^2_ν	R_{Ag-Ag} (Å)	$S_0^2(Ag-Ag)$	σ^2_{Ag-Ag} (Å^2)
HF	11.0	2.88 ± 0.01	0.59	$0.0024 \pm 1 \times 10^{-4}$
HL	34.1	2.88 ± 0.01	0.98	$0.0027 \pm 1 \times 10^{-4}$

obtained results [16]. However, the value of the reduction factor $S_0^2(Ag-Ag) = 0.98$, obtained under the fixed number of Ag nearest neighbors $N = 12$ in foil by HL-potential, seems to be overestimated for intrinsic losses in transition metals [19,20]. Therefore, in the following the HF backscattering amplitudes and phase shifts, together with the fixed value of $S_0^2(Ag-Ag) = 0.59$ will be used in IFEFFIT for the structural analysis of Ag nanoparticles in as prepared and annealed soda-lime glasses.

Fig. 4 compares $F(R)$ of Ag K-edge EXAFS in the reference Ag foil at $T = 10$ K, obtained for the used truncated Δk, to those of the single-shell fit (a) and of the fit (b), which takes into account five coordinating shells of the absorbing Ag atom (where each shell was represented by a single-scattering path) added with the scattering path of the focusing effect on the first and the "shadowed" fourth shells in *fcc* structure [22]. Fig. 4(b) illustrates that these scattering paths of Ag *fcc* structure reproduce the $F(R)$ features in the extended R-range. The corresponding fit exhibits stability of the values of the structural parameters for the first shell of Ag in Ag foil presented in Table 1 and illustrates that the effect of MS processes on the values of these parameters within this Δk interval is negligible.

The dotted blue curve in Fig. 4(b) illustrates the $F(R)$ of the averaged $\chi(k)$, calculated by FEFF8 [23] for the absorbing Ag atoms located at the nonequivalent surface positions of Ag cluster with radius 5.8 Å. The cluster has the *fcc* structure for the interior atoms. Calculations of $\chi(k)$ were performed by the same approximation for the photoelectrons scattering processes that was used for the dashed red curve of Fig. 4(b), and making changes ($\leq$0.2 Å) of interatomic Ag–Ag distances in the vicinity of the absorbing atom. This simulation gives the reduction of magnitude of peaks in $F(R)$ of the surface Ag atom contribution and the minor changes in R-positions of these peaks, retaining in general the *fcc* behavior of $F(R)$ in the extended R-range up to ~6.5 Å, if we do not create any significant ($\geq$0.05 Å) structural distortions in the vicinity of the absorbing Ag atom in the near-surface region.

One more advantage of the used Δk interval with $k_{min} = 6.5$ Å^{-1} is the diminishing of the effect of Ag – O bonds in glass on the determined Ag–Ag parameters. This is explained by the low contribution of Ag – O backscattering amplitudes in the higher k-range in comparison with Ag–Ag ones, which is reflected in the envelopes of corresponding $\chi(k)$ functions, calculated for two scattering paths Ag–12Ag with $R_{Ag-Ag} =$ 2.89 Å and Ag–2O with $R_{Ag-O} =$ 2.17 Å, presented in Fig. 5(a). The diminishing of Ag – O effect on the determined Ag–Ag parameters by such a choice of k_{min} was confirmed by the FT analysis of the simulated function $\chi_{model}(k)$ compiled as a sum of experimental $\chi^{experim}_{Ag-foil}(k)$ of Ag foil and calculated Ag–2O contribution $\chi^{theor}_{Ag-2O}(k)$ of Fig. 5(a). Fig. 5(b) compares $F(R)$ of this $k\chi_{model}(k)$ with that of the single-shell Ag–Ag fit, where FT was performed over the Δk interval: $k_{min} = 6.5$ Å^{-1}, $k_{max} =$ 14.0 Å^{-1}. The use of the $k_{min} = 6.5$ Å^{-1} and corresponding fit gave the same values of Ag–Ag structural parameters for the first shell of Ag in Ag foil as those presented in Table 1.

This simulation shows that if $F(R)$ of Ag K-edge EXAFS is obtained by the truncated Δk interval started from k_{min} ~ 6.5 Å^{-1} then the contribution of Ag – O bonds in glass is negligible and determination of Ag–Ag structural parameters for Ag(1) and Ag(2) states in soda-lime glass

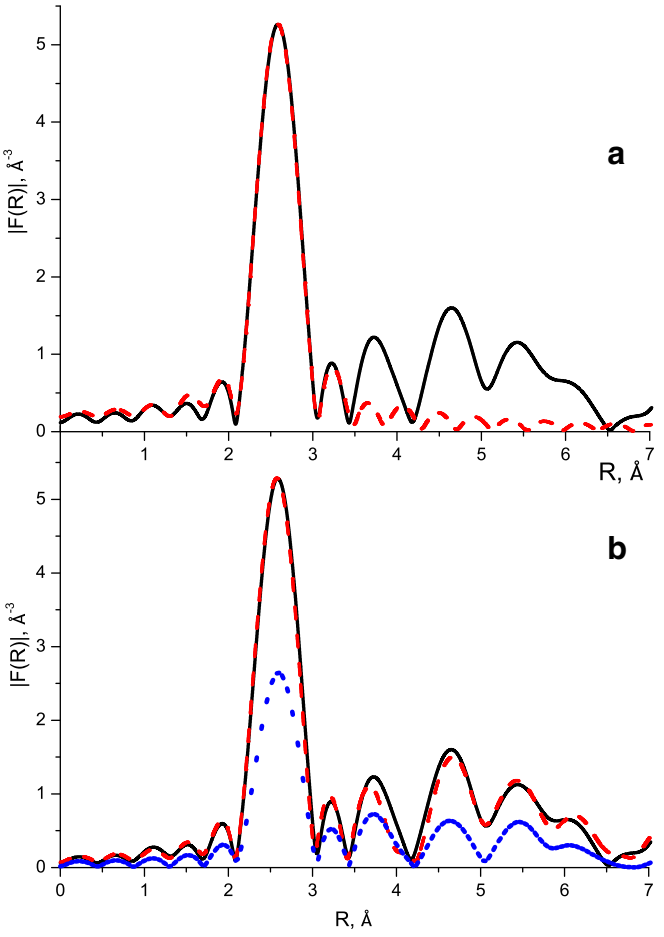

Fig. 4. FT magnitudes $F(R)$ obtained by $k_{min} = 6.5$ Å^{-1} and $k_{max} = 14.0$ Å^{-1}. Solid black curves– $F(R)$ for $k^2\chi(k)$ of experimental Ag K-edge EXAFS in Ag foil at $T = 10$ K; dashed red curves—results of the fits based on different approximations for the local structure of the absorbing Ag, placed in the center of *fcc*–cluster with radius 5.8 Å: (a)—only one shell around the absorbing Ag is considered within the single-scattering approach, (b)—photoelectron single-scattering on five nearest shells of the absorbing Ag added with the focusing effect on the first and "shadowed" fourth shells of *fcc* structure. Dotted blue curve in (b)—averaged contribution of the absorbing Ag atoms, placed at the nonequivalent positions on the surface of the chosen Ag-cluster.

can be performed by the fit based on the function $\chi_{model}(k)$ obtained from Eq. (4):

$$\chi_{\text{model}}(k) = C_1\chi_{Ag(1)}(k) + C_2\chi_{Ag(2)-Ag(2)}(k). \quad (6)$$

The second refinement of the fitting procedure helps to overcome strong correlations between the number of variable amplitude parameters, which result in instabilities of the fit, ambiguities in the fit parameters and in the determined models of nanoparticle structure. The choice of a model based solely on χ^2_ν or F-test [24] is therefore difficult or impossible, and often has a high probability of obtaining nonphysical values of parameters.

These difficulties can at least partially be overcome by taking into account that correlations in amplitude parameters are differently manifested at different k-weightings of $\chi(k)$ and different Δk intervals used for FT. The differences in manifestation of correlations effect enable to suggest the technique for their diminishing via the generalization of the well known scheme for the choice of the two correlating parameters values. The scheme uses the crossing region of interdependency of these two parameters, obtained at differently weighted $k^n\chi^{experim}(k)$ ($n = 0, 1, 2$). The suggested generalization is

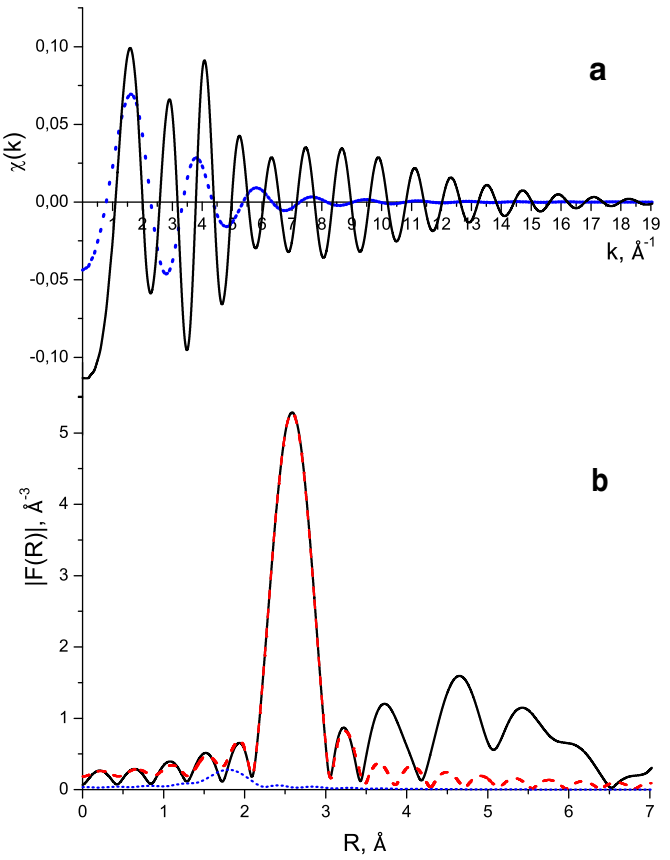

Fig. 5. (a)—Comparison of χ(k) calculated for scattering paths Ag–12Ag (solid black curve) and Ag–2O (dotted blue curve); (b)—comparison of FT magnitudes $F(R)$ of $k^2\chi_{model}(k) = k^2(\chi^{experim}_{Ag-foil}(k) + \chi^{theor}_{Ag-2O}(k))$ (solid black curve) obtained by the truncated Δk interval ($k_{min} = 6.5$ Å^{-1}, $k_{max} = 14.0$ Å^{-1}) with corresponding function of the single-shell Ag–Ag fit (dashed red curve). Dotted blue curve in (b) shows the magnitude of Ag–2O contribution in $F(R)$ within the used Δk interval.

based on the use of interdependency of all of the correlating parameters of the signal, obtained both at different weights k^n and at different Δk intervals. In this approach, the region of the amplitude parameters stability, which corresponds to minimal correlations among them, was chosen as the result of the crossing of m-dimensional surfaces (m is the number of correlating parameters), where each surface corresponds to defined values of Δk interval and of weight k^n ($n = 0, 1, 2$).

These surfaces were obtained by systematic variation of the correlating parameters, ensuring that all possible structural models (including the ones, which give not the best fit quality, but provide the values of variable parameters in their physically reasonable boundaries) are included into the comparative analysis. The stepped variation of parameters was done by the package IncrementalFIT, which enables repeated triggering of IFEFFIT with step-wise change of some of the input parameters.

The third refinement also significantly improves the stability of the fitting procedure for Ag nanoparticles and implies the use of a fixed contribution $\chi^{experim}_{Ag-foil}(k)$ for the first term in Eq. (1) or in Eq. (6). This function $\chi^{experim}_{Ag-foil}(k)$ was obtained from experimental Ag K-edge EXAFS in Ag foil and hence, contains the exact contributions from the first and more distant shells of a Ag(1) atom in the core of the nanoparticle. The inclusion of $\chi^{experim}_{Ag-foil}(k)$ as a fixed contribution into the fit by IFEFFT can be easily done via small replacements in the input file feff000*i*.dat which contains the photoelectron backscattering amplitudes and phase shifts [21], where the number i must correspond to Ag(1) state. In this scheme, the function $\chi_{Ag(1)}(k)$ in Eq. (6) was constructed as $\chi_{Ag(1)}(k) = \chi^{experim}_{Ag-foil}(k) * \exp(-2 * \Delta\sigma^2_{Ag(1)}k^2)$, where multiplication by the factor $\exp(-2 * \Delta\sigma^2_{Ag(1)}k^2)$ was made to account for the difference in structural order in the first shell of Ag atom in a nanoparticle with that in the foil, within the R-range of the first shell. For Ag foil $\Delta\sigma^2_{Ag(1)}$ equals zero by definition.

The term $\chi_{Ag(2)}(k)$ in Eq. (6) was approximated by the single-scattering expression [25] and the number of variables needed to describe it was diminished by setting the value of the amplitude reduction factor $S_0^2(Ag-Ag)$ for the near-surface Ag-atoms equal to that in Ag foil. However, because S_0^2 for Ag foil correlates with σ^2, to reduce this correlation different dependencies $\left\{\sigma^2\left(S_0^2\right)\right\}_{k^n,(\Delta k)_i}$ were obtained from the experimental Ag K-edge EXAFS in Ag foil under differently weighted functions $k^n\chi(k)$ ($n = 0, 1, 2$) and for different Δk_i intervals ($i = 1$ corresponds to 5.0–14.0 Å^{-1} and $i = 2$ to 6.5–14.3 Å^{-1}) for FT and compared according to our second refinement for the fitting procedure. The corresponding curves for Ag foil at $T = 10$ K gave the crossing region $\left\{\sigma^2\left(S_0^2\right)\right\}_{k^n,(\Delta k)_i} \cap \left\{\sigma^2\left(S_0^2\right)\right\}_{k^p,(\Delta k)_j}$ centered at the following values of parameters: $\sigma^2_{Ag-Ag} = 0.0024$ Å^2 and $S_0^2(Ag-Ag) = 0.59$, which were presented in Table 1. The value of $S_0^2(Ag-Ag) = 0.59$ is used in the following study of Ag nanoparticles atomic structure in soda-lime glasses.

4. Results

To study atomic structure of silver nanoparticles in as prepared and annealed glasses at $T = 10$ K the fit of $F(R)$ of experimental Ag K-edge EXAFS was performed by Eq. (6) using the technique of Section 3 with $k_{min} \sim 6.5$ Å, the variables C_1 and $\Delta\sigma^2_{Ag(1)}$ for the term $\chi_{Ag(1)}(k)$. The contribution of the near-surface Ag(2) atoms was given by the function $C_2\chi_{Ag(2)-Ag(2)}(k)$ in Eq. (6) with the variable C_2 and was approximated by the single-shell term in the single-scattering form [25], with the averaged structural parameters: $<N_{Ag(2)}>$—mean number of nearest neighbors for Ag(2) atom, $\sigma^2_{Ag(2)-Ag(2)}$—mean DW parameter for Ag(2)–Ag(2) correlation, $<R_{Ag(2)-Ag(2)}>$—mean interatomic distance between nearest Ag(2) atoms, and energy parameter $E_0(Ag(2))$ [25]. As was mentioned above, the fits with these variables were ambiguous and unstable because of the correlation between the amplitude parameters C_1, $\Delta\sigma^2_{Ag(1)}$, $C_2 <N_{Ag(2)}>$, $\sigma^2_{Ag(2)-Ag(2)}$. To diminish these correlations, the technique of Section 3 was applied to functions $F(R)$ of differently weighted oscillatory parts $k^n\chi(k)$ ($n = 0, 1, 2$) of Ag K-edge EXAFS, obtained for different $(\Delta k)_i$ intervals (i numbers the intervals with k_{min} changed from 6.0 to 7.5 Å^{-1} and k_{max} changed by ± 0.5 Å^{-1} in relation to 14.0 Å^{-1} for as prepared and in relation to 18.5 Å^{-1} for annealed samples). For each of these $F(R)$ functions the fit was performed by the stepped variation of parameters C_1 (from 0.00 to 1.00, step 0.01), $\Delta\sigma^2_{Ag(1)}$ (from 0.0000 to 0.0050 Å^2, step 0.0001), $C_2 <N_{Ag(2)}>$ (from 0.0 to 12.0, step 0.01) and varying one amplitude parameter $\sigma^2_{Ag(2)-Ag(2)}$ and parameters $<R_{Ag(2)-Ag(2)}>$, $E_0(Ag(2))$. As a result, we have obtained the four-dimensional surfaces $\left\{\sigma^2_{Ag(2)-Ag(2)}\left(C_1, \Delta\sigma^2_{Ag(1)}, C_2\langle N_{Ag(2)}\rangle\right)\right\}_{k^n,(\Delta k)_i}$, where each surface corresponds to one defined value of k^n and $(\Delta k)_i$. The crossing region of these surfaces corresponds to the reduced correlation between the four amplitude parameters, and was determined by the unbiased sample dispersion [26] of $\sigma^2_{Ag(2)-Ag(2)}$ with an accuracy of ~0.0005 Å^2.

Determining the values of correlating amplitude parameters by this scheme and employing refinements in the fitting procedure described in Section 3, diminished significantly any ambiguity in obtained results, improved their stability and provided the choice of Ag nanoparticles structure by the criteria [27] based on the χ^2_ν and F-test values. Corresponding Ag–Ag structural parameters are presented in Table 2.

Table 2 shows that the values of $\Delta\sigma^2_{Ag(1)}$ are negligible (≤ 0.001 Å^2) for Ag nanoparticles both in as prepared and annealed glasses. Together with the results of Figs. 2(b) and 4(b) this unambiguously indicates that Ag atoms in the core region of these nanoparticles have the local structure which corresponds to *fcc* structure of Ag-foil. Table 2 shows also the

increase of $<R_{Ag(2)-Ag(2)}>$ in the near surface region of nanoparticles from 2.85 Å in as prepared sample to 2.89 Å in the annealed one (the last value coincides with that of the interior region within the accuracy of R determination). This increase is probably caused by the diminishing of the number of defects in the near surface region after annealing, because the presence of such defects leads to the decrease of the number of nearest neighbors of atom and as a result—the shortening of interatomic distances.

One can see that the annealing of as prepared soda-lime glass, results in the increase of the percentage C_1 of such a Ag(1) atoms by ~17%. The accuracy of C_1 determination by the F-test is ~7% (using the $S_0^2(Ag-Ag)$ and $E_0(Ag(1))$ values of the reference Ag foil) and cannot be improved because of the remaining correlations between parameters C_1 and $\sigma^2_{Ag(2)-Ag(2)}$. Meanwhile, for Ag nanoparticles in both as prepared and annealed glasses the values of structural parameters C_2 $<N_{Ag(2)}>$ and $<R_{Ag(2)-Ag(2)}>$, as well as the value of energy parameter $E_0(Ag(2))$ for the near-surface region of nanoparticle, exhibited remarkable stability upon the inaccuracies in C_1 determination. Moreover, the value of $E_0(Ag(2))$ also slightly differs ($\leq$2 eV) between nanoparticles in as prepared and annealed samples.

The structural Ag–Ag parameters of Table 2 are independent of Ag – O interactions and therefore were used then as the fixed ones to determine the Ag – O parameters in as-prepared and annealed samples at $T = 10$ K by the extended Δk-intervals: from $k_{min} = 2.8$ Å^{-1} to $k_{max} = 14.0$ Å^{-1} for as prepared and to $k_{max} = 18.0$ Å^{-1} for the annealed ones. The demonstration of Ag – O contributions within these intervals is illustrated by Fig. 6(a,b), which shows the F(R) of $k\chi(k)$ of experimental Ag K-edge EXAFS in as prepared and annealed samples in comparison with corresponding theoretical functions, calculated by the fixed Ag–Ag parameters of Table 2, without inclusion of Ag – O contribution into the structural model. The significance of Ag – O contribution is clearly visible at $R \leq 2.2$ Å.

The parameters of Ag – O bonds were determined using the extended Δk intervals, started from k_{min} ~ 2.8 Å^{-1}, and the fit performed by Eq. (4) with the variables $R_{Ag(3)-O}$, $\sigma^2_{Ag(3)-O}$ and C_{Ag-O}, under the fixed values of Ag–Ag parameters of Table 2 and $S_0^2(Ag-O) = 0.83$ for Ag – O path [28]. The last was determined by experimental Ag K-edge EXAFS in the reference crystalline AgO [29] using HF scattering amplitudes and phase shifts.

The following C_{Ag-O} values were obtained: for as prepared sample $C_{Ag-O} = 0.57$ and for annealed one $C_{Ag-O} = 0.42$. For these samples Fig. 6(c,d) show the agreement in the extended R-range (up to ~6 Å) between $F(R)$ of $k\chi(k)$ of experimental Ag K-edge EXAFS and corresponding functions obtained by this fit with Ag – O interaction included into the model. This comparison permits to conclude that the disagreement in the low R-range ($\leq$2.2 Å) at Fig. 6(a,b) between theoretical curves and the ones of experimental spectra can be attributed to the contribution of Ag – O bonds not included into the fit model.

In section "Supplementary material" it is shown that for both as prepared and annealed samples the values of C_1, C_2 $<N_{Ag(2)}>$ of Table 2 together with the obtained values of C_{Ag-O} enabled to conclude that the term $C_2\widetilde{C}_2/2$ in Eq. (5) is within the accuracy of C determination ($\leq$7%). Therefore instead of Eq. (5) one can use:

$$C_{Ag-O} \approx C_3$$

which means that the main contribution of Ag – O bonds arise from a large amount of Ag(3) atoms in as prepared and annealed glasses.

The obtained C_1 and C_3 values for as prepared and annealed samples were used then to determine the corresponding values of C_2 by Eq. (2). The last ones were used at the final step of the analysis to determine $<N_{Ag(2)}>$ from the values of C_2 $<N_{Ag(2)}>$ of Table 2. The application of this procedure gave the resulting structural parameters for Ag(1), Ag(2) and Ag(3) states in as prepared and annealed soda-lime glasses collected in Table 3. The presented values were determined together with the values of other fitting parameters: ΔE_0 $(Ag(2)-Ag(2)) = -3.2 \pm 0.5$ (eV) for the term $\chi_{Ag(2)-Ag(2)}(k)$, ΔE_0 $(Ag(3)-O) = -5.1 \pm 0.5$ (eV) for the term $\chi_{Ag(3)}(k)$ using the back-scattering amplitudes and phase shifts of HF MT-potential model, and using the fixed values of the reduction factors $S_0^2(Ag-Ag) = 0.59$ and $S_0^2(Ag-O) = 0.83$ obtained above by these HF amplitudes and the reference bulk compounds.

5. Discussion

Table 3 shows that the obtained value of $R_{Ag(3)-O}$ is very close to the earlier obtained value [10] and the XRD value for crystalline AgO (2.176 Å [30]) in contrast to $R_{Ag-O} = 2.061$ Å in Ag_2O [31].

For as prepared sample the low value of C_1 (11%) and the value of C_2 (32%) show that Ag nanoparticles in this sample have a very small core region with *fcc* structure and the main part of Ag atoms in nanoparticle belongs to its near-surface region. This in turn indicates for a very small size of Ag nanoparticles in as prepared sample, while the amount of Ag atoms in Ag(3) states is large (C_3 ~ 57%). The TEM study of as prepared sample [10] revealed the absence of strong deviations in the dispersion of the particles sizes. In this case the particle mean size D was estimated using the approximate dependence of D upon the ratio C_1/C_2. This dependence, presented in Fig. 7, was theoretically obtained for our case using the cluster model of nanoparticle, which assumes that *fcc* local structure of the core is continued up to its surface. The used estimate gave for as prepared sample the value of $D \sim 1.4 \pm 0.5$ nm, which is within the boundaries suggested by TEM [10].

In as prepared sample the value of the mean interatomic Ag(2)–Ag(2) distance in the near-surface region of Ag nanoparticles is noticeably smaller than that in the annealed one, while the last coincides with $R_{Ag(1)-Ag(1)}$ in the core region of nanoparticle and in Ag foil. Taking into account also the large enough value of $\sigma^2_{Ag(2)-Ag(2)}$ (compared to that for the core) at such a temperature, one can conclude that in the small Ag nanoparticles the mean interatomic Ag(2)–Ag(2) distance in the near-surface region is shortened and there is a significant variation in $R_{Ag(2)-Ag(2)}$ values, which indicates for the modification of the near-surface region of *fcc* particles.

In the annealed sample, the averaged size of Ag nanoparticles increases according to the significant increase of the ratio C_1/C_2 from 0.35 in as prepared sample to 0.93. The TEM investigations [10] revealed the presence of a few very large particles with sizes up to ~30–40 nm besides of a lot of smaller ones. This is probably the reason of slight increase of $\sigma^2_{Ag(2)-Ag(2)}$ compared to as prepared sample, since as was mentioned earlier the large surfaces of such particles are usually characterized by the increasing concentration of defects in the near surface region. These large particles contribute both into the C_1 and C_2 values and

Table 2
Structural Ag–Ag parameters for the core and for the near-surface regions of Ag nanoparticles in as prepared and annealed soda-lime glasses at T = 10 K, determined by the fitting technique of Section 3 applied to Ag K-edge EXAFS.

Samples	Core of Ag nanoparticle (Ag(1) atoms)		Near-surface region of Ag nanoparticle (Ag(2) atoms)		
	C_1	$\Delta\sigma^2_{Ag(1)}$ (Å^2)	C_2 $<N_{Ag(2)}>$	$\sigma^2_{Ag(2)-Ag(2)}$ (Å^2)	$<R_{Ag(2)-Ag(2)}>$ (Å)
As prepared	0.11 ± 0.07	$0.0001 \pm 1 \times 10^{-4}$	2.14 ± 0.07	$0.0037 \pm 1 \times 10^{-4}$	2.85 ± 0.01
Annealed	0.28 ± 0.07	$0.0001 \pm 1 \times 10^{-4}$	2.66 ± 0.07	$0.0043 \pm 1 \times 10^{-4}$	2.89 ± 0.01

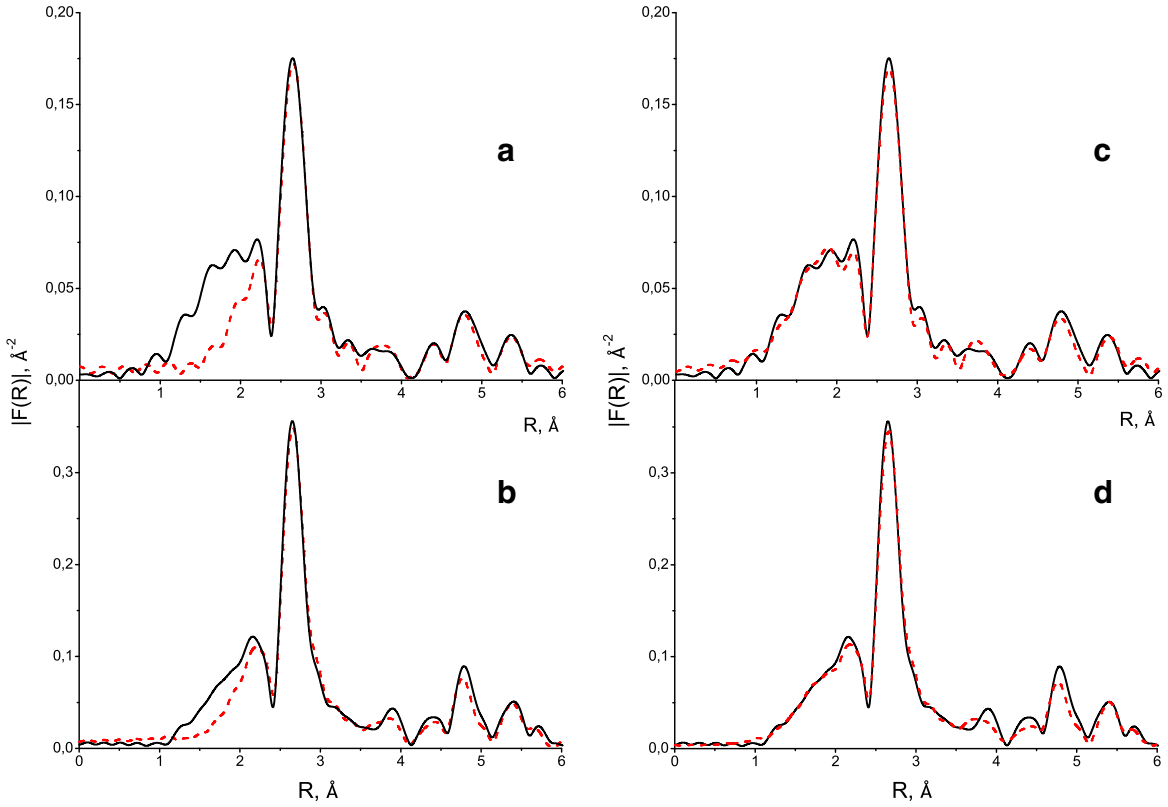

Fig. 6. FT magnitudes $F(R)$ of $k\chi(k)$ of experimental Ag K-edge EXAFS (solid black curves) in as prepared (a), (c) and annealed (b), (d) samples compared to corresponding theoretical functions (dashed red curves) calculated by the fixed Ag–Ag parameters of Table 2 without Ag – O contribution—(a),(b) and by the fit with the fixed Ag–Ag parameters of Table 2, taking into account Ag – O contribution into the fitting model—(c), (d). FT of spectra was performed by the extended Δk-intervals, starting from $k_{min} = 2.8\,Å^{-1}$.

hence one may expect that the obtained value of C_1/C_2 ratio is less adequate for the nanoparticles structure and size characterization. Nevertheless, because of the very small number of these large particles, the same estimate of the mean size D of nanoparticles, that was used for as prepared sample, was performed for the annealed one which gave the value of $D \sim 2.5 \pm 0.7$ nm in reasonable correlation with TEM data.

The revealed increase of the mean size of nanoparticles and simultaneous decrease of the C_3 value (to 42%) in the annealed sample suggested the two mechanisms of nanoparticles size growth: i) agglomeration of existing in as prepared sample small Ag nanoparticles and ii) reduction of silver ions in Ag(3) states and formation of new nuclei of Ag particles with their following agglomeration.

6. Conclusions

The study of features formation in the extended R-range of $F(R)$ of Ag K-edge EXAFS in Ag foil at $T = 10$ K and determination of atomic structure of silver nanoparticles in as prepared and annealed soda-lime glasses at the same temperature, performed by the proposed scheme of FT and refinements of the fitting technique, provided the results which can be summarized as follows:

- if the FT of experimental Ag K-edge EXAFS in Ag foil is performed by $k_{min} \sim 6.5\,Å^{-1}$ ($E \sim 25.663$ keV) then the features of $F(R)$ in the extended R-range (up to ~6.5 Å) are reproduced by taking into account the photoelectron single scattering on the first five shells around the absorbing Ag atom and the focusing effect on the linear scattering path through the atoms of the first and "shadowed" fourth shells in *fcc* structure. Thus truncated Δk interval provides the same accuracy of the first shell Ag–Ag structural parameters in Ag foil as the extended interval with $k_{min} = 2.8\,Å^{-1}$;
- $F(R)$ of the averaged contribution of the absorbing Ag atoms, located at the nonequivalent positions on the surface of cluster with *fcc* local structure of the core, differ from that of Ag-foil mainly by the significant (up to ~two times for the cluster's size $D \sim 1.2$ nm) reduction in the magnitudes of peaks under their stable positions and the conserved general form of $F(R)$ in the extended R-range, if we do not create any significant (≥ 0.05 Å), structural distortions in the vicinity of the absorbing Ag atom in the near-surface region;

Table 3
Structural parameters for Ag(1), Ag(2) and Ag(3) states of silver atoms in as prepared and annealed samples at $T = 10$ K.

Samples of glass	Ag(1)	Ag(2)				Ag(3)		
	C_1	C_2	$<R_{Ag(2)-Ag(2)}>$ (Å)	$<N_{Ag(2)}>$	$\sigma^2_{Ag(2)-Ag(2)}$ (Å^2)	C_3	$R_{Ag(3)-O}$ (Å)	$\sigma^2_{Ag(3)-O}$ (Å^2)
As prepared	0.11 ± 0.07	0.32 ± 0.07	2.85 ± 0.01 Å	6.6 ± 1.5	$0.0037 \pm 1 \times 10^{-4}$ Å^2	0.57 ± 0.07	2.17 ± 0.01 Å	$0.0073 \pm 1 \times 10^{-4}$ Å^2
Annealed	0.28 ± 0.07	0.30 ± 0.07	2.89 ± 0.01 Å	8.9 ± 2.0	$0.0043 \pm 1 \times 10^{-4}$ Å^2	0.42 ± 0.07	2.17 ± 0.01 Å	$0.0070 \pm 1 \times 10^{-4}$ Å^2

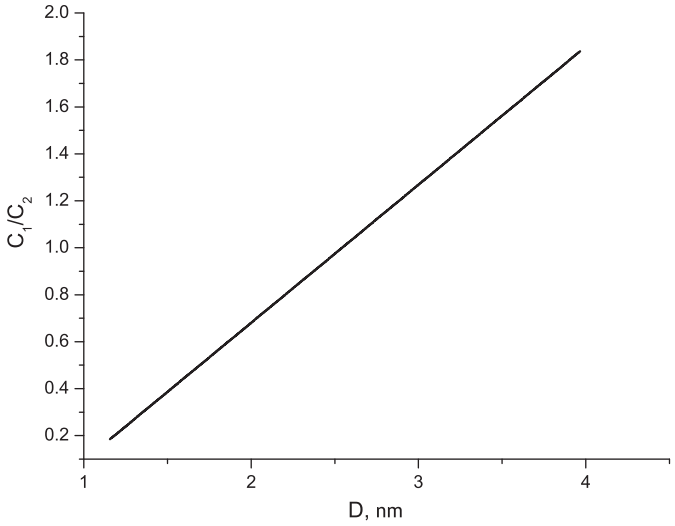

Fig. 7. Dependence of the ratio C_1/C_2 upon the particle mean size D, theoretically obtained under the assumption that *fcc* local structure of the interior region is continued up to the surface of the chosen atomic cluster.

- the proposed refinements of the fitting technique enabled to overcome instabilities of the standard approach of the FT analysis of Ag K-edge EXAFS, caused by the various species of the absorbing Ag atom in the sample, and to go beyond the averaged description of silver nanoparticles structure to more detailed study, which gave the atomic structure of their core, the structural characteristics of the near-surface region and Ag–O bonding, the percentage of Ag atoms in each of these species before and after annealing process;
- the local structure of Ag atoms in the core region of silver nanoparticles in both as prepared and annealed soda-lime glasses is similar to that of the *fcc* structure of Ag foil. However, in as prepared sample the core region and the size of the whole nanoparticle are small (the last was estimated as $D \sim 1.4 \pm 0.5$ nm), while approximately the half of Ag atoms in the sample are bonded with two oxygen atoms;
- the annealing of as prepared glass at $T = 823$ K during 8 h resulted in the increase of the core region and the mean size of Ag nanoparticles (the last up to $D \sim 2.5 \pm 0.7$ nm) and the reduction of the number of Ag atoms bonded with two oxygen ones. The mechanism of Ag nanoparticles growth in soda-lime glasses under the thermal treatment was suggested.

The proposed technique of the fit is particularly promising for identification of the core–shell structure in noble and transition atoms' bimetallic nanoparticles.

Acknowledgments

The work was supported by grant No. 213.01-24 of the Southern Federal University (RF).

Appendix A. Supplementary data

Supplementary data to this article can be found online at http://dx.doi.org/10.1016/j.jnoncrysol.2013.09.025.

References

[1] S.I. Bozhevolnyi, N.L. Kildeby, O.Z. Andersen, R.E. Røge, T. Larsen, R. Petersen, J.F. Riis, Silver Nanoparticles, Institute for Physics and Nanotechnology, Aalborg University Project Group N344, 2005.
[2] V. Torres, M. Popa, D. Crespo, J.M. Calderón Moreno, Microelectron. Eng. 84 (2007) 1665–1668.
[3] R.M. Mohamed, I.A. Mkhalid, J. Alloys Compd. 501 (2010) 301–306.
[4] M. Dubiel, S. Brunsch, W. Seifert, H. Hofmeister, G.L. Tan, Eur. Phys. J. D16 (2001) 229–232.
[5] H.-E. Mahnke, I. Zizak, P. Schubert-Bischoff, V. Koteski, Mater. Sci. Eng. 149 (2008) 200–203.
[6] H. Masafumi, I. Yasuhiro, N. Masaharu, J. Colloid Interface Sci. 337 (2009) 427–438.
[7] K.P. Bankura, D. Maity, M.R. Mollick, D. Mondal, B. Bhowmick, M.K. Bain, A. Chakraborty, J. Sarkar, K. Acharya, D. Chattopadhyay, Carbohydr. Polym. 89 (2012) 1159–1165.
[8] G.A. Sotiriou, A. Teleki, A. Camenzind, F. Krumeich, A. Meyer, S. Panke, S.E. Pratsinis, Chem. Eng. J. 170 (2011) 547–554.
[9] G. Cao, Nanostructures and Nanomaterials, Imperial College, W., 2004
[10] R. Schneider, M. Dubiel, J. Haug, H. Hofmeister, AIP Conf. Proc. 882 (2007) 743.
[11] M. Dubiel, S. Brunsch, S. Kolb, D. Gutwerk, H. Bertagnolli, J. Non-Cryst. Solids 220 (1997) 30.
[12] A.I. Gusev, Nanomaterials, Nanostructures, Nanotechnologies, Fizmatlit, M., 2005. 416.
[13] M.G. Newville, Ph.D Thesis, University of Washington, 1995. 81–106.
[14] L.A. Bugaev, L.A. Avakyan, V.V. Srabionyan, A.L. Bugaev, Phys. Rev. B 82 (2010) 064204.
[15] E.D. Crozier, J.J. Rehr, R. Ingals, X-ray Absorption: Principles, Applications, Techniques of EXAFS, SEXAFS and XANES, Wiley, N.Y., 1988
[16] J. Haug, A. Chassé, R. Schneider, H. Kruth, M. Dubiel, Phys. Rev. B 77 (2008) 184115.
[17] M. Newville, B. Ravel, D. Haskel, J.J. Rehr, E.A. Stern, Y. Yacoby, Physica B 208&209 (1995) 154.
[18] L.A. Bugaev, R.V. Vedrinskii, I.G. Levin, V.M. Airapetian, J. Phys. Condens. Matter 3 (1991) 8967.
[19] I.B. Borovskii, R.V. Vedrinskii, V.L. Kraizman, V.P. Sachenko, Usp. Fiz. Nauk 149 (1986) 27.
[20] M. Roy, S.J. Gurman, G. van Dorssen, J. Phys. 7 (1997) 151.
[21] M. Newvville, IFEFFIT web page and online documentation, http://cars9.uchicagj.edu/ifeffit.
[22] L.A. Bugaev, R.V. Vedrinskii, I.G. Levin, Physica B 158 (1989) 378.
[23] A.L. Ankudinov, B. Ravel, J.J. Rehr, S.D. Conradson, Phys. Rev. B 58 (1998) 7565.
[24] L. Downward, C.H. Booth, W.W. Lukens, F. Bridges, AIP Conf. Proc. 882 (2007) 129.
[25] E.A. Stern, X-ray Absorption: Principles, Applications, Techniques of EXAFS, SEXAFS and XANES, Wiley, N.Y., 1988
[26] D.C. Montgomery, G.C. Runger, Applied Statistics and Probability for Engineers, Wiley, N.Y., 1994
[27] A. Filipponi, A. Di Cicco, Phys. Rev. B 52 (1995) 15135.
[28] J.J. Rehr, J.J. Kas, M.P. Prange, A.P. Sorini, L.W. Campbell, F.D. Vila, AIP Conf. Proc. 882 (2007) 85.
[29] http://cars9.uchicago.edu/svn/demeter/trunk/lib/Demeter/share/standards/data.
[30] J.A. McMillan, J. Inorg. Nucl. Chem. 13 (1960) 28.
[31] R.W.G. Wyckoff, Crystal Structures, Second edition Wiley, N.Y., 1963.